ICES Journal of Marine Science Advance Access published January 18, 2009

Seasonal and interannual variability of primary and export production in the South China Sea: a three-dimensional physical–biogeochemical model study

Guimei Liu and Fei Chai

Liu, G., and Chai, F. 2009. Seasonal and interannual variability of primary and export production in the South China Sea: a three-dimensional physical–biogeochemical model study. – ICES Journal of Marine Science, 66.

To investigate the seasonal and interannual variations in biological productivity in the South China Sea (SCS), a Pacific basin-wide physical–biogeochemical model has been developed and used to estimate the biological productivity and export flux in the SCS. The Pacific circulation model, based on the Regional Ocean Model Systems (ROMS), is forced with daily air–sea fluxes derived from the NCEP (National Centers for Environmental Prediction) reanalysis between 1990 and 2004. The biogeochemical processes are simulated with a carbon, $Si(OH)_4$, and nitrogen ecosystem (CoSiNE) model consisting of silicate, nitrate, ammonium, two phytoplankton groups (small phytoplankton and large phytoplankton), two zooplankton grazers (small micrograzers and large mesozooplankton), and two detritus pools. The ROMS–CoSiNE model favourably reproduces many of the observed features, such as Chl *a*, nutrients, and primary production (PP) in the SCS. The modelled depth-integrated PP over the euphotic zone (0–125 m) varies seasonally, with the highest value of 386 mg C m^{-2} d^{-1} during winter and the lowest value of 156 mg C m^{-2} d^{-1} during early summer. The annual mean value is 196 mg C m^{-2} d^{-1}. The model-integrated annual mean new production (uptake of nitrate), in carbon units, is 64.4 mg C m^{-2} d^{-1}, which yields an *f*-ratio of 0.33 for the entire SCS. The modelled export ratio (*e*-ratio: the ratio of export to PP) is 0.24 for the basin-wide SCS. The year-to-year variation of biological productivity in the SCS is weaker than the seasonal variation. The large phytoplankton group tends to dominate over the smaller phytoplankton group, and likely plays an important role in determining the interannual variability of primary and new production.

Keywords: export flux, modelling, primary and new production, South China Sea.

Received 5 September 2007; accepted 8 December 2008.

G. Liu and F. Chai: University of Maine, School of Marine Sciences, 5706 Aubert Hall, Orono, ME 04469, USA. G. Liu: Institute of Oceanology, Chinese Academy of Sciences, Qingdao, 266071, China. Correspondence to F. Chai: tel: +1 207 5814317; fax: +1 207 5814388; e-mail: fchai@maine.edu.

Introduction

The South China Sea (hereafter referred to as the SCS), with an area of 3 500 000 km^2, is a semi-closed marginal sea in the western part of the North Pacific Ocean (0–25°N 100–125°E; Figure 1). It consists of extended continental shelves and a deep basin. The water is generally shallow (<61 m) throughout the vast northwestern and southwestern continental area of the sea, including the Gulf of Tonkin, Gulf of Thailand, and Sunda shelf. In contrast, the abyssal SCS basin in the northeast reaches depths >5000 m. The SCS is bounded by the Malay Peninsula and the Southeast Asian mainland to the west, Taiwan to the north, the Philippines to the east, and Borneo to the south. The SCS is isolated from the western Pacific Ocean by a chain of islands, and exchanges between the SCS and the North Pacific Ocean take place via many channels among those islands, primarily through Taiwan Strait, Luzon Strait, Mindoro Strait, and Karimata Strait (Xue *et al.*, 2004; Fang *et al.*, 2005). The Luzon Strait, with a sill at 2200 m, forms the only deep connection between the western North Pacific Ocean and the SCS, so the physical and chemical properties remain essentially constant below 2200 m in the SCS (Metzger and Hurlburt, 1996; Chen *et al.*, 2001). The Kuroshio, which forms the western boundary current of the subtropical gyre in the North Pacific, penetrates the SCS through the Luzon Strait seasonally (Xue *et al.*, 2004). All the other straits have water depths <100 m, so heat and salt exchanges are limited. Outflow is primarily through the Taiwan Strait in the north all year-round. The other weak flows vary seasonally through the Mindoro Strait to the east and the wide Karimata Strait to the south (Xue *et al.*, 2004).

Despite these complexities in water exchange, the SCS is an ideal natural laboratory to study the relationship between climate variability and marine ecosystem response. The SCS is located between the Tibetan Plateau and the West Pacific Warm Pool (WPWP), where the dominant climate signal is related to the strong seasonality of the East Asia Monsoon. In summer, the southwesterly monsoon starts in June and lasts until August, whereas in winter, the northeasterly monsoon starts in October and dominates into early spring (Chu and Fan, 2001). Transition periods are in April and May for the southwesterly monsoon, and in September for the northeasterly monsoon. The alternating monsoons in winter and summer modify the circulation in the SCS (Wu *et al.*, 1998; Su, 2004; Xue *et al.*, 2004). The

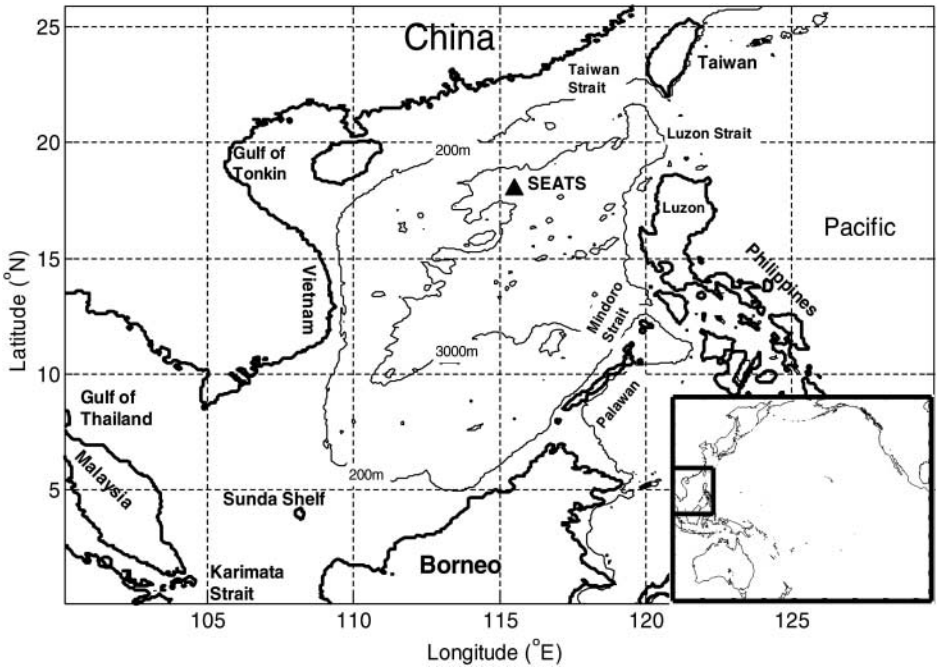

Figure 1. Map of the SCS. The triangle shows the location of the SouthEast Asian Time-series Station (SEATS).

basin-wide circulation pattern displays a large cyclonic gyre, which persists throughout the year in the northern portion of the SCS. The circulation in the southern portion is predominantly cyclonic in winter and anticyclonic in summer (Takano *et al.*, 1998; Wu *et al.*, 1998; Chai *et al.*, 2001a; Su, 2004; Wang *et al.*, 2005). Beyond the seasonal time-scale, the SCS circulation also exhibits interannual variation related to *El Niño*/Southern Oscillation events (Chao *et al.*, 1996; Wu *et al.*, 1998; Kuo *et al.*, 2004; Fang *et al.*, 2006; Rong *et al.*, 2006; Straub *et al.*, 2006).

Biogeochemical processes in the SCS have been documented and are linked to changes in atmospheric forcing and water circulation. For example, biological responses to the alternating monsoon winds have been studied in the SCS and its subregions (Yin, 2002; Tang *et al.*, 2004; Ning *et al.*, 2004; Chen *et al.*, 2006a, b). Because of limited spatial and temporal observation coverage, key biological processes, such as primary production (PP, total carbon uptake by phytoplankton), new production, respiration, and downward flux of particulate materials, have not been fully investigated in the SCS. This limitation adds further uncertainty to any regional or global production and carbon flux estimation. Using an NPZD, four-component, nitrogen-based, physical–biological model with 0.4° horizontal resolution and 21 vertical layers, Liu *et al.* (2002) showed that the southerly wind in summer favours high Chl *a* concentrations off the east coast of Vietnam. Conversely, northerly wind in winter favours high nutrients, Chl *a*, and PP off the west coast of Luzon Island. However, long-term variability in primary and export production has not been explored.

In this context, we use a three-dimensional physical–biogeochemical model to estimate the biological productivity and export flux in the SCS seawards of the 50-m isobath. The overall goals are to elucidate quantitatively the primary and export production in the SCS basin (excluding the extended continental shelves) and associated seasonal and interannual variations. Our work is organized as follows. The physical–biogeochemical model (ROMS–CoSiNE) is outlined, then model and data comparisons are given. Modelled seasonal and interannual variations of biological productivity are then discussed, followed by summary and concluding remarks.

Physical–biogeochemical model

The physical model for this study is based on the Regional Ocean Model Systems (ROMS), which represents an evolution in the family of terrain-following vertical-coordinate models. It solves the primitive equations with hydrostatic and Boussinesq approximations. ROMS contains innovative algorithms for advection, pressure-gradient force, free-surface variations, and *K*-profile vertical-mixing parameterizations for surface and bottom boundary layers (Large *et al.*, 1994; Shchepetkin and McWilliams, 1998, 2003). Wang and Chao (2004) configured a ROMS circulation model for the Pacific Ocean (45°S–65°N 99°E–70°W) at 50-km horizontal resolution and 20 vertical levels, with realistic geometry and topography. For this modelling study, we followed Wang and Chao's (2004) approach. The coarse grid of $5^\circ \times 5^\circ$ is shown in Figure 1, but each coarse grid consists of 10×10 subgrid cells in the model. In the regions near the two closed northern and southern walls, a sponge layer with a region of 5° from the walls is applied for temperature, salinity, and nutrients. The treatment of the sponge layer consists of a decay term $\kappa(T^\star - T)$ in the temperature equation [$\kappa(S^\star - S)$ for the salinity equation, $\kappa(N^\star - N)$ for the nutrient equation], which restores predictions to the observed temperature $T^\star$ (salinity $S^\star$, nutrients $N^\star$) field at the two closed walls. The value of κ varies smoothly from $1/30\ \mathrm{d}^{-1}$ at the walls to zero 5° away from them.

The biogeochemical model is based on the carbon, $Si(OH)_4$, and nitrogen ecosystem (CoSiNE) model developed by Chai *et al.* (2002) and Dugdale *et al.* (2002) (Figure 2). The CoSiNE model includes silicate, nitrate, ammonium, two phytoplankton groups, two zooplankton grazers, and two detritus pools. In Figure 2, P1 represents small, easily grazed phytoplankton whose

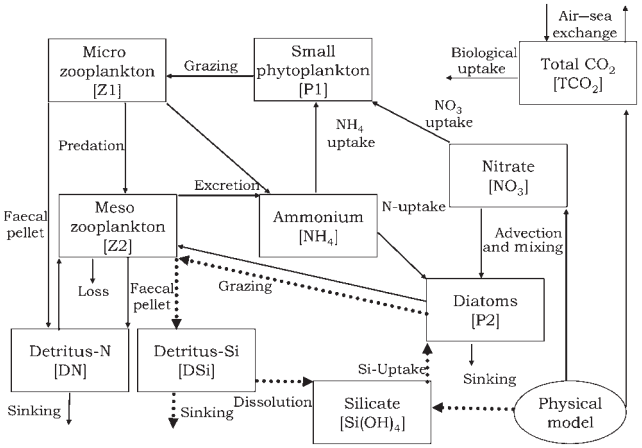

Figure 2. Diagram of the carbon, $Si(OH)_4$, nitrogen ecosystem (CoSiNE) model, depicting the inter-compartmental flow chart of the ecosystem and linkage to physical processes in the euphotic zone. The flow of nitrogen is indicated by solid lines and the flow of silicon by dotted lines.

specific growth varies, but whose biomass is regulated by micrograzers (Z1) and whose daily net productivity is largely remineralized (Chavez *et al*., 1991; Landry *et al*., 1995, 1997). P2 represents large diatom-like phytoplankton (>10 mm in diameter) that form high-biomass blooms and contribute disproportionately to sinking flux as ungrazed production or large faecal pellets (Smetacek, 1985; Bidigare and Ondrusek, 1996). The large diatom-like phytoplankton has the potential to grow fast under optimal nutrient conditions (using the Michaelis–Menten constant for nutrient uptake; Coale *et al*., 1996). Z1 represents small micrograzers whose specific growth rate is similar to P1 phytoplankton, and whose grazing rate is density-dependent (Landry *et al*., 1997). Z2 represents larger mesozooplankton that graze on diatoms and detritus nitrogen (DN), and prey on Z1. The detritus pool is split into DN and detritus silicon (DSi) to balance supplies of nitrogen and silicon through upwelling and vertical mixing separately. DSi is given a vertical sinking velocity of 10 m d^{-1} in the model, and sinks faster than DN. The linkage of the carbon cycle to the ecosystem model is through the consumption and remineralization of assimilated nutrients based on nitrogen changes in the water column combined with Redfield stoichiometric ratios. The modelled Chl *a* concentration is derived from the phytoplankton biomass concentration (mmol-N m^{-3}), converted to mg m^{-3} using a nominal ratio of gramme chlorophyll to molar nitrogen of 1, corresponding to a chlorophyll to carbon mass ratio of 1/50 and a C/N molar ratio of 7.3 (Thomas and Dodson, 1972; Anderson and Sarmiento, 1994; Chai *et al*., 2007).

Below the euphotic zone, sinking particulate organic matter is converted to inorganic nutrients by a regeneration process similar to that used by Chai *et al*. (1996), in which organic matter decays to ammonium and is then nitrified to nitrate.

The CoSiNE model has been used in studies of decadal variability in PP of the North Pacific (Chai *et al*., 2003). Recently, it has been coupled with ROMS for the Pacific basin-scale configuration. Initialized with climatological temperature, salinity, and nutrients from the World Ocean Atlas (WOA) for 2001 (Ocean Climate Laboratory National Oceanographic Data Center, 2002), the Pacific ROMS–CoSiNE model has been forced with the climatological air–sea fluxes calculated using the bulk formula for several decades to reach quasi-equilibrium.

From this quasi-equilibrium, we integrated the ROMS–CoSiNE model for the period 1990–2004 and force it with daily air–sea fluxes of momentum, heat, and fresh water derived from the NCEP/NCAR (National Centers for Environmental Prediction/National Center for Atmospheric Research) reanalysis (Kalnay *et al*., 1996). The surface windstress is calculated from the 10-m wind based on the Large and Pond (1982) drag coefficient formulation. The heat flux is calculated from the prescribed short- and long-wave radiations, and sensible and latent heat fluxes are calculated by the bulk formula with prescribed air temperature and relative humidity. The fresh-water flux is derived from the prescribed precipitation, and evaporation is derived from the latent heat release. It has been reported that water from the nutrient-poor Mekong River, one of the largest rivers of the SCS, does not fertilize the phytoplankton growth in the Vietnam upwelling region (Dippner *et al*., 2007). For the current model configuration, the river discharges are not included. The biological model is initialized using the January nitrate and silicate profiles of the WOA for 2001 (Ocean Climate Laboratory National Oceanographic Data Center, 2002). After the initial spin-up period of 20 years forced by the climatological physical condition in 1989, the biological model runs from 1 January 1990 through 31 December 2004. The monthly-averaged results are used in the analysis, focusing on the period 1990–2004.

Comparing model results with observations

SouthEast Asian Time-series Study (SEATS) data, initiated in September 1998 by the National Center for Ocean Research (NCOR), Taiwan (Wong *et al*., 2007), were used to evaluate the model results. Detailed descriptions of the measured Chl *a*, nitrate, and silicate concentrations can be found elsewhere (Gong *et al*., 1992; Tseng *et al*., 2005, 2007). Nutrient and chlorophyll profiles for comparison were only available from September 1999 to July 2000.

Sea surface temperature and sea surface salinity

To evaluate the physical model performance, we compared the modelled sea surface temperature (SST) and sea surface salinity (SSS) with observations at the SEATS site taken at 3-month intervals from October 2000 to October 2003. Temperature varied from 24°C to 31°C at the SEATS site (Figure 3a), with pronounced seasonal and interannual variations. The differences between the modelled SST and the observational data were <0.5°C. The ROMS–CoSiNE model captures the basic variability of SST at the SEATS site both in terms of magnitude and phase, but the model shows multiple small peaks during the period of comparison. Xie *et al*. (2003) documented semi-annual variations of SST in the SCS with satellite data. Higher temporal resolution would be required to validate the subseasonal SST variability found in the model results. The ROMS–CoSiNE modelled SSS are within the same range as the observations at the SEATS site from 2000 to 2003 (Figure 3b). The modelled SSS ranged from 32.6 to 34.4 and had similar seasonal and interannual variations to the SSS observed at the SEATS site. The differences between observed and modelled SSS were <0.5. Overall, the interannual variability of the simulated SST and SSS exhibits similar features to the observations.

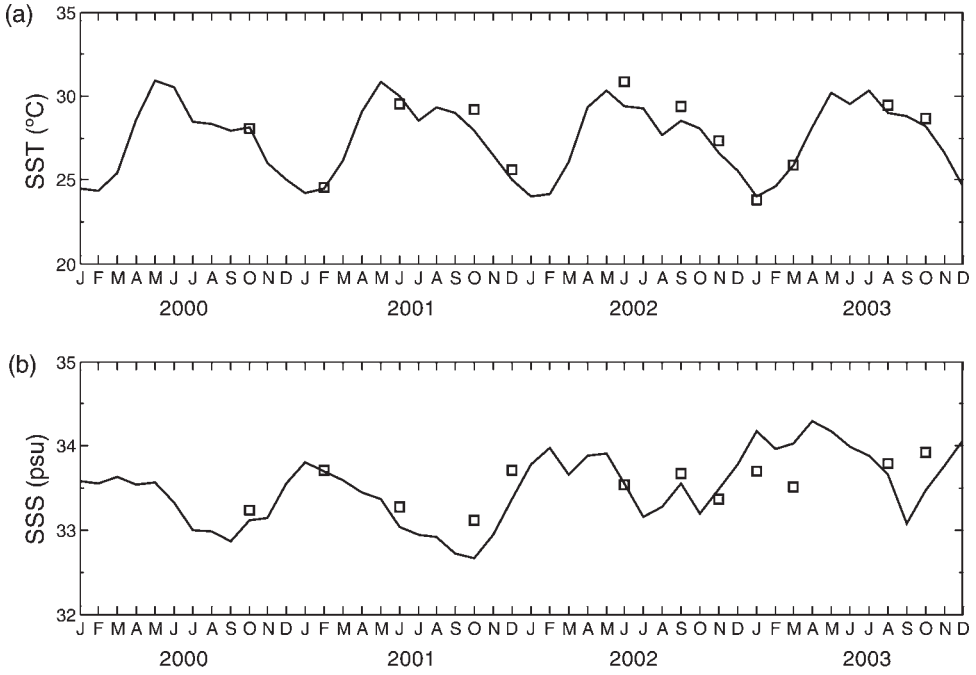

Figure 3. Comparison of modelled (a) sea surface temperature (SST) and (b) sea surface salinity (SSS), with the SEATS observational data from 2000 to 2003. Lines are model predictions, open squares are observations.

Volume transports

Model predictions of volume transport were compared with observations in the region of the Luzon Strait, because that area dominates the inflow from the Pacific into the SCS. It is recognized that the Kuroshio intrudes into the SCS through the Luzon Strait in winter, but there is debate whether the Kuroshio intrudes during summer (Wyrtki, 1961; Qu, 2000; Liang *et al.*, 2003). The model-simulated seasonal variation and annual mean volume transport across the Luzon Strait were calculated to compare with observations, and to assess the potential seasonal dynamics in volume transport.

The modelled annual mean transport and seasonal variation agree with previous estimates made by the dynamic computation method and from acoustic Doppler current profiler (ADCP) observations (Qu, 2000; Liang *et al.*, 2003). On an annual mean basis, the model predicts a net inflow into the SCS through the Luzon Strait of 2.9 Sv (1 Sv $= 10^6$ m^3 s^{-1}; the positive value indicates that the flow enters the SCS). Depending on the method and period of observations, previous studies showed a wide range of estimates for transport through Luzon Strait (Metzger and Hurlburt, 1996, 2001; Qu, 2000; Liang *et al.*, 2003; Fang *et al.*, 2005). Fang *et al.* (2005) provided a summary of the annual mean volume transport through the Luzon Strait, which ranges from 0.1 to 8.0 Sv. Using the dynamic computation method (based on the sea level difference across Luzon Strait), Qu (2000) estimated an annual mean volume transport of 3.0 Sv. The long-term (1991–2000) mean volume transport through the Luzon Strait estimated from the ADCP array (0–300 m) is 3.0 Sv (Liang *et al.*, 2003). Liang *et al.* (2003) also confirmed that the Kuroshio flowed into the SCS steadily and persistently, even in summer when the southwest monsoon season prevails.

Based on the model output from 1990 to 2004, the water from the Pacific enters the SCS through the Luzon Strait with pronounced seasonal variability. The transport across the Luzon Strait is stronger in winter and weaker in summer, with a maximum of 6.3 Sv in November and 5.3 Sv in December, and a minimum of 1.0 Sv in April and 1.6 Sv in July. These predictions are similar to estimates based on observations that indicate maximum volume transport (5.3 Sv) in January/February and minimum transport (0.2 Sv) in June/July (Qu, 2000). The seasonal variation in the transport across the Luzon Strait is similar to the model results of Xue *et al.* (2004), but there is a 1-month lag.

Phytoplankton biomass, nutrients, and PP

We evaluate the ROMS–CoSiNE performance of biological components by comparing the modelled results with the observations at the SEATS site. We apply the same dataset from SEATS used by Liu *et al.* (2002) to compare observed vertical profiles of Chl *a*, nitrate, and PP with the ROMS–CoSiNE model predictions, then determine how well the model predicts nitrate and silicate using all available data (September 1999 to July 2000).

The ROMS–CoSiNE model reproduces the observed Chl *a* and nitrate concentration profiles reasonably well, but predicted Chl *a* concentrations were lower at the surface for observations in March 2000 (Figure 4). The Chl *a* concentration is in the range 0.1–0.5 mg m^{-3} in the water column (Figure 4a). The model produces a vertical profile of nitrate similar to the observations (Figure 4b), but the simulated concentration is higher than observations deeper than 40 m. This could be the result of higher upward nitrate flux from vertical upwelling and stronger background diffusion.

The modelled profile of PP in March is similar to observations, but it underestimates PP $<$ 15 m and suggests a subsurface maximum at 30 m that is not evident in the data (Figure 4c). The modelled PP is calculated based on the nutrient uptake by both small and large phytoplankton groups, converted to carbon units using a constant C/N ratio of 7.3. The difference between model predictions and observations may result from the use of

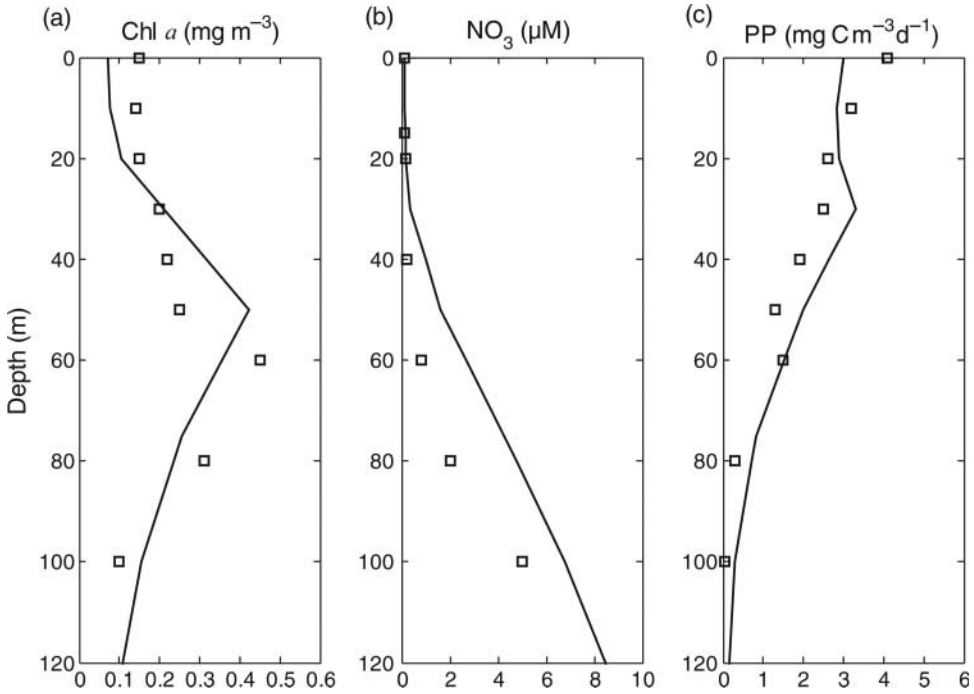

Figure 4. Comparison of modelled (a) Chl *a*, (b) nitrate, and (c) PP (solid lines) with observational data (squares) at the SEATS site in March 2000 (after Liu *et al.*, 2002).

the fixed C/N ratio of 7.3 used in the model. In the SCS, the observed C/N ratios range from 5.5 to 11.4 (Liu *et al.*, 2007).

Additional model-data comparisons of vertical profiles of Chl *a*, nitrate, and silicate in January and July 2000 show that the model reproduces the observed Chl *a* profile reasonably well in January 2000 (Figure 5a), but that the modelled subsurface Chl *a* maximum at 60 m in July 2000 is lower than the observations (Figure 5d). The model predictions compare favourably with observed nitrate and silicate concentrations in both January and July 2000 (Figure 5b, c, e, and f).

Modelled nitrate and silicate compare well with all available observations at the SEATS site. Bimonthly observations (from September 1999 to July 2000) are used in a linear regression with modelled nitrate and silicate concentrations (Figure 6). The slopes for nitrate and silicate are close to 1, and high r^2 values are obtained (0.99 for nitrate and silicate). In the euphotic zone

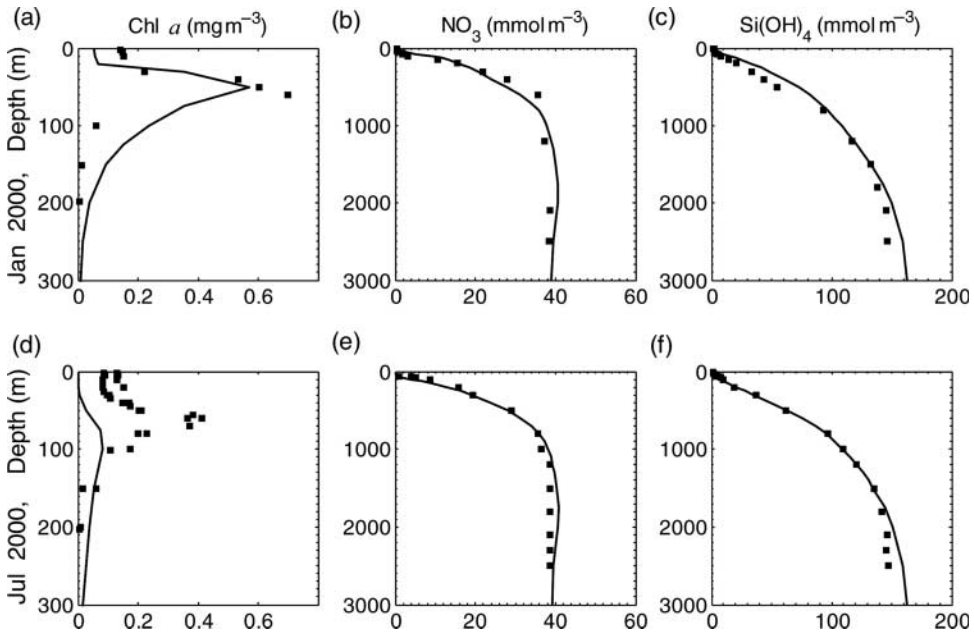

Figure 5. Comparison of modelled (a and d) Chl *a*, (b and e) nitrate, and (c and f) silicate with observational data in (a–c) January 2000 and (d–f) July 2000 at the SEATS.

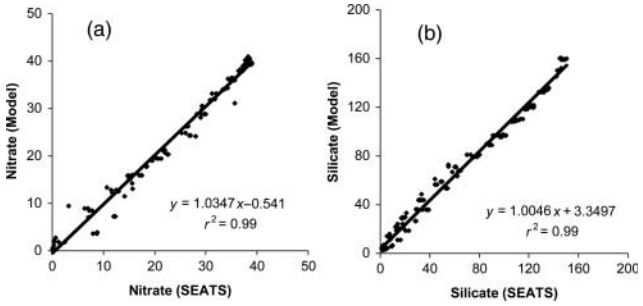

Figure 6. Model predictions plotted against bimonthly SEATS observations of (a) nitrate (mmol-N m^{-3}) and (b) silicate (mmol-Si m^{-3}) from September 1999 to July 2000.

where the water depth is shallower than 100 m, r^2 values for nitrate and silicate are 0.77 and 0.72, respectively.

Our limited model-data comparison captures the basic physical and biological processes that regulate SST, SSS, Chl *a*, nitrate, and PP at a location where observations are available. Discrepancies between model output and observations could result from a number of factors, including model error or inadequate observational sampling. For example, the relatively coarse horizontal (50 km) and vertical (20 levels) resolution could result in inadequate representation of circulation patterns and mixed-layer dynamics, and, subsequently, the biological response. Moreover, the model uses a constant conversion factor between phytoplankton biomass and Chl *a*, which should vary depending on light and nutrient conditions (Geider *et al.*, 1998). However, as a first-order comparison, the model reproduces the general vertical profile of Chl *a*, which suggests that the model captures large-scale and mean conditions of the key physical and biological processes in the SCS.

Biological productivity and export flux in the SCS

After gaining confidence in model simulations, we used the ROMS–CoSiNE model results to evaluate the primary and export production in the SCS and to elucidate their seasonal and interannual variations.

Seasonal variation in biological productivity and export flux

The model results from January 1990 to December 2004 were averaged by month to create a monthly mean climatology, which illustrates seasonal variations of the basin-scale depth-integrated PP (IPP), depth-integrated new production (INP) over the euphotic zone between the surface and 125 m, and particulate organic carbon (POC) export flux at 125-m depth.

The modelled IPP experiences strong seasonal variation comparable with the observations, varying between 156 and 386 mg C m^{-2} d^{-1} (Figure 7). The IPP is higher during winter and early spring (December–March), and there is another small peak of IPP in late summer (August/September). The lowest values of IPP are in June and November. The modelled seasonal variation of IPP is similar to the results obtained by Liu *et al.* (2002), who reported that the IPP is high in winter and ranges from 207 to 373 mg C m^{-2} d^{-1}. Some limited observations of IPP throughout the northern SCS (113–120°E 18–23°N) also show higher values in winter (January) and early spring (March), and lower levels in early summer (June and July), with

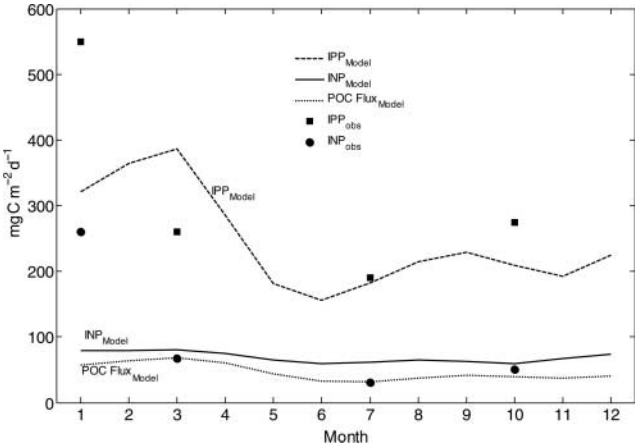

Figure 7. Monthly mean values of depth-integrated PP (IPP_{Model}), depth-integrated new production (INP_{Model}), and POC export flux ($POC\ Flux_{Model}$) at 125 m based on the model results from 1990 to 2004 at the regions with depth greater than 125 m, The observed mean IPP_{obs} (black squares) and INP_{obs} (dots) at sampling stations throughout the northern SCS were obtained from Chen (2005).

slight increases in autumn (October; Chen, 2005; Figure 7). The mean of these observed IPPs is higher than the modelled IPP in January and October, but lower than the model results in March. This difference could have resulted from the strong year-to-year variation in IPP (Chen, 2005), which is smoothed in model results by monthly averaging.

Compared with the IPP, the modelled INP shows little seasonal variability and is in the range 55–76 mg C m^{-2} d^{-1}, except in January (Figure 7; note the conversion from nitrogen units to carbon units with a constant C/N ratio of 7.3). The observed mean INP in the northern SCS is 140 ± 80 mg C m^{-2} d^{-1} in March and 110 ± 60 mg C m^{-2} d^{-1} in October (Chen, 2005). The averaged mean observed INP from 2000 to 2003 is higher than the modelled IPP in January, but lower than that in March, July, and October (Figure 7). The model results overestimate the INP slightly compared with the observations.

In addition to evaluating the biological productivity and carbon flux, we also examine the nitrate balance in the SCS. The upward nitrate flux is estimated as the modelled vertical velocity multiplied by nitrate concentration at a fixed depth, which is 125 m in our study. The modelled annual mean of vertical nitrate flux across 125 m for the SCS is 0.78 mmol-N m^{-2} d^{-1}, which is closely balanced with the modelled INP of 0.74 mmol-N m^{-2} d^{-1} (in nitrogen units). This indicates that the model conserves the nitrate budget on an annual mean basis, at least for the nitrate influx to the euphotic zone and phytoplankton uptake.

Export flux of POC is also quantified. The modelled seasonal POC export flux at 125 m varies slightly, with a range of 30–70 mg C m^{-2} d^{-1} (Figure 7). Percentage-wise, the interannual variability of POC export flux follows that of IPP (Figure 7). Our modelled domain-averaged POC export flux at 125 m is 46.5 mg C m^{-2} d^{-1} in the SCS, comparable with the estimates of POC flux derived from observed data and model estimates made by Liu *et al.* (2002). Based on the normalized depth-dependent function of POC flux observed near Hawaii (Martin *et al.*, 1987) and the POC flux value at 1000 m reported by Jennerjahn *et al.* (1992), Liu *et al.* (2002) calculated the expected

POC flux at 125 m to be 42 mg C m^{-2} d^{-1}, and their modelled mean flux at 125-m depth to be 48 mg C m^{-2} d^{-1} from September to March in the SCS.

The *f*-ratio and the *e*-ratio

Model predictions are used to calculate *f*- and *e*-ratios. The *f*-ratio is defined as the fraction of total PP fuelled by nitrate, which indicates contributions of nitrate and ammonium uptake (new vs. regenerated production) in the total nitrogen uptake. The model-derived *f*-ratio agrees with observations and indicates that biological productivity in the SCS is dominated by regenerated production. The modelled annual mean values for the basin-scale averaged IPP, INP, and regenerated production (total uptake of NH_4 by both phytoplankton groups and converted to carbon unit) are 196.4, 64.4, and 132 mg C m^{-2} d^{-1}, respectively. According to these values, the *f*-ratio obtained is 0.33 (*f*-ratio = INP/IPP = 64.4/196.4), close to the observed values of 0.28 $\pm$ 0.08 (March 2001 and 2002) and 0.32 $\pm$ 0.14 (October 2002) in the northern SCS (Chen, 2005). The low *f*-ratio obtained from both the model and observations shows that the biological productivity is dominated by regenerated production in the SCS. Some two-thirds of the PP in the SCS is derived from recycled nitrogen, demonstrating that a significant quantity of organic carbon and nitrogen has been cycled through zooplankton grazing in the euphotic zone.

Similar to the *f*-ratio, the *e*-ratio measures the fraction of the POC export flux in the total PP. Based on the modelled PP and export production, the export ratio (*e*-ratio) is obtained as POC export flux (46.5)/IPP (196.4) = 0.24. The low *e*-ratio value indicates that most of the organic carbon produced in the euphotic zone is respired. Only ~24% of the newly produced organic carbon is exported vertically to deep water (>125 m) as POC. It is reported that the *e*-ratio has an inverse relationship with temperature for the world's oceans (Laws *et al*., 2000; Fujii *et al*., 2005). In tropical and subtropical waters with high temperature (>20°C), e.g. the Bermuda Atlantic Time-series Study (BATS), the Hawaii Ocean Timeseries (HOT), and in the Arabian Sea, *e*-ratios tend to be at the lower end of the range, often between 0.08 and 0.15. However, in upwelling regions or at higher latitudes with relatively low temperatures (<16°C), e.g. at Station P in the Gulf of Alaska, off the coast of Peru, and in the Ross Sea, the *e*-ratio is much higher, with values of 0.4–0.7. The SCS is located in the subtropical region with annual-averaged water temperatures between 22°C and 25°C, and its model-estimated *e*-ratio is therefore comparable with other regions of high temperature (>20°C).

Spatial patterns in the seasonal variation of biological productivity and export flux

As biological productivity and biomass vary greatly from region to region depending on nutrient and light conditions in the SCS (Tang *et al*., 2004), model predictions were used to assess the spatial variation of biological productivity and export flux. The modelled distribution of IPP and POC export flux at 125 m in January and July and the annual mean are presented in Figure 8. In January, the modelled IPP develops from the inner shore off Luzon Island to the outer shelf is high in the eastern SCS and low in the western SCS (Figure 8a). The highest predicted value of IPP is ~1000 mg C m^{-2} d^{-1}, and the simulated domain-averaged IPP is 321 mg C m^{-2} d^{-1}. In July, the domain-averaged IPP is 182 mg C m^{-2} d^{-1} (Figure 8b), lower than the annual mean value of 247 mg C m^{-2} d^{-1} (Figure 8c). High modelled IPP in July is located near the coast off Vietnam and extends to the outer shelf, and lower IPP in the eastern SCS (Figure 8b). The spatial patterns of the modelled IPP respond to upwelling along the Vietnam coast, which is attributable to the southwesterly monsoon of summer (Dippner *et al*., 2007). The intense coastal upwelling brings nutrients to the surface to sustain higher PP. The modelled high IPP off the Vietnam coast coincides with the high Chl *a* region in the SeaWiFS-derived Chl *a* distributions in summer reported by Zhao and Tang (2007). There could be some differences between the model and satellite results because the satellite-derived values only include the top 10–15 m, whereas the modelled IPP is integrated over the euphotic zone. The modelled highest value of annual mean IPP is >600 mg C m^{-2} d^{-1} in the SCS. The model indicates highest IPP at the Sunda Shelf on an annual mean basis, but decreasing from low latitudes to high latitudes (Figure 8c).

The sinking of particulate organic material is an important pathway for linking surface productivity and the recycling of the elements below. The modelled distribution of POC export flux at 125 m tends to follow the distribution of IPP, with higher export carbon flux corresponding to regions with enhanced PP. The POC export flux at 125 m is high in the southeastern part of the SCS in winter (Figure 8d) and in the southwestern SCS in summer (Figure 8e). Mirroring the modelled annual mean distribution of the IPP, the annual mean horizontal distribution of POC export flux at 125 m is high in the south and low in the north (Figure 8f). The POC export flux is in the range 0–180 mg C m^{-2} d^{-1}, less than one-fifth of the IPP. Based on a relationship between the particulate beam attenuation coefficient and POC concentration, Gardner *et al*. (2006) derived the averaged POC concentration over one attenuation depth. Their results indicate that the averaged POC concentration in the upper ocean is 36–60 mg m^{-3} in summer and 48–72 mg m^{-3} in winter. Although there can be a large difference in POC concentration between the euphotic zone average (estimated from satellites) and that at the base of the euphotic zone (estimated with the model), both model predictions of POC export flux and remote-sensing-estimated POC concentrations indicate that there is seasonal variation, with high values in winter and low values in summer in the SCS.

The temporal and spatial variations in the modelled PP and POC export flux show close relationships with upwelling dynamics. Upwelling off Luzon Island in winter and off Vietnam in summer have been recognized and studied from previous circulation models and remote-sensing studies (Chao *et al*., 1996; Shaw *et al*., 1996; Chai *et al*., 2001b; Xie *et al*., 2003; Wu and Chang, 2005; Dippner *et al*., 2007). The dominant mechanisms attributed to the winter and summer upwelling in the SCS are monsoons, coastline angle, bathymetry, local windforcing, and Kuroshio intrusion. Shaw *et al*. (1996) also suggested that upwelling contains a large, remotely forced component arising from the basin circulation, such that a northward undercurrent can cause the upward movement of water in winter. Therefore, strong upwelling along the eastern side of the SCS during winter could lead to large vertical nutrient transport to the surface layer and could stimulate phytoplankton productivity which is high in the eastern SCS in winter (Liu *et al*., 2002). During summer, PP and POC export flux are at their highest levels off Vietnam. General circulation patterns are driven by the spatial asymmetry in monsoon forcing in summer and are characterized by an upwelling-induced northward undercurrent and a recently detected southward countercurrent

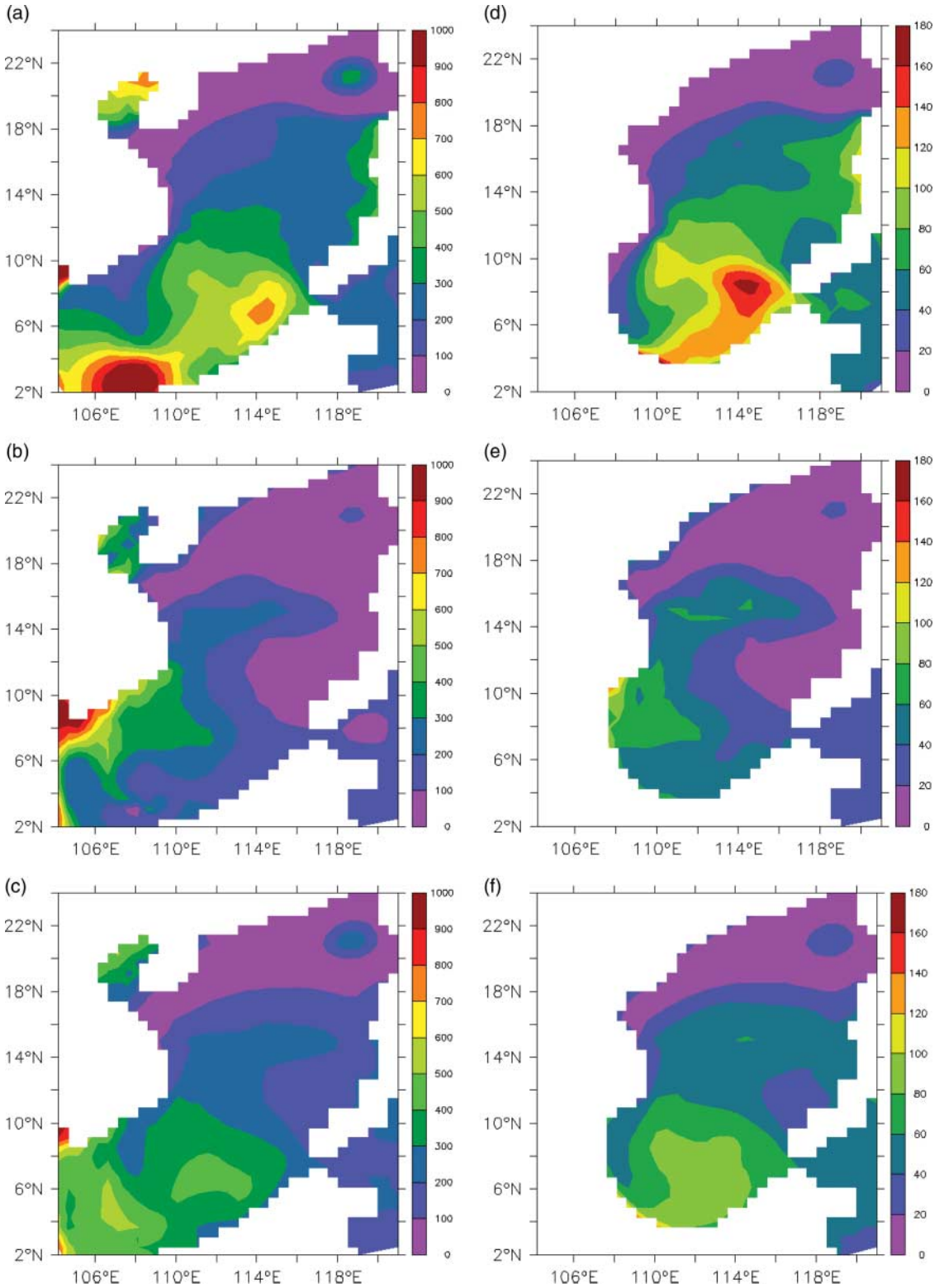

Figure 8. Spatial patterns in depth-integrated (0 – 125 m) PP in (a) January, (b) July, and (c) the annual mean, and POC export flux at 125 m in (d) January, (e) July, and (f) the annual mean, based on the model results from 1990 to 2004. Units are mg C m^{-2} d^{-1}.

(Dippner *et al.*, 2007). The resulting deformation of this flow pattern forms an offshore jet around 12°N, and local enhancement of the upwelling intensity (Dippner *et al.*, 2007), which subsequently enhances biological productivity. Dippner *et al.* (2007) stated that phytoplankton growth in the area was fertilized by nutrient-rich upwelling water attributable to upwelling dynamics rather than by the input of nutrient-poor river water. Our model predictions capture the spatial patterns in phytoplankton

production associated with upwelling dynamics in the SCS and suggest that nutrient transport and nutrient availability in the euphotic zone determine biological productivity in the SCS.

Interannual variation of biological productivity and phytoplankton assemblages

The SCS experiences strong interannual variation attributable to the changes in sea surface forcing and exchanges between the SCS and the Pacific Ocean (He *et al*., 1997; Rong *et al*., 2006).

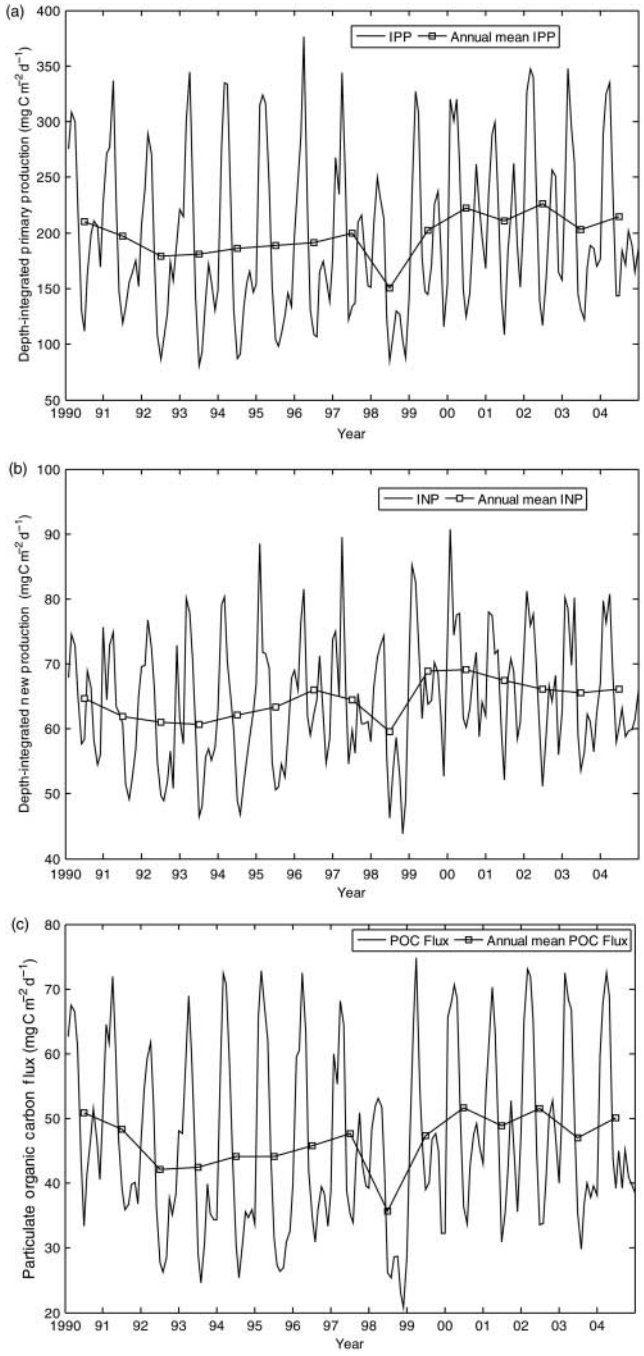

Figure 9. Model predictions of (a) domain-averaged IPP and its annual mean, (b) INP and its annual mean, and (c) POC export flux at 125 m and its annual mean. Results were calculated using predictions from the regions with depths >125 m.

Model predictions of biological productivity in the SCS also are characterized by strong interannual variation (Figure 9). For example, the modelled IPP is 377 mg C m^{-2} d^{-1} in March 1996, but only 130 mg C m^{-2} d^{-1} in March 1998. IPP, INP, and POC export flux at 125 m, averaged over the model domain, varied between 81 and 377 mg C m^{-2} d^{-1}, 44 and 91 mg C m^{-2} d^{-1}, and 21 and 75 mg C m^{-2} d^{-1}, respectively, from 1990 to 2004. There is a seasonal double peak in IPP each year from 1990 to 2004, with modelled INP and POC export flux at 125 m following the increasing/decreasing trend of IPP to a certain extent. Although these results suggest some noteworthy trends, they need to be confirmed by long-term field observations.

Small and large phytoplankton functional groups can make different contributions to the total PP and POC export flux. Model results indicate that large diatom-like phytoplankton (P2) at the surface, at 125 m, and depth-averaged over the euphotic zone (0–125 m) constitute 53, 99, and 82%, respectively, of the phytoplankton community biomass (Figure 10a). Both P1 and P2 are more abundant in winter and less so in late summer (Figure 10b), in agreement with the observation that the proportion of diatoms in the total phytoplankton biomass varied from 95.7% in winter to 75.9% in summer (Ning *et al*., 2004). Near the surface, the modelled P1 and P2 are about equal in terms of their contributions to total phytoplankton biomass (Figure 10b), whereas P2 is the dominant phytoplankton group at 125 m. Model results suggest that, over the whole water column, small phytoplankton (P1) contribute less than large phytoplankton (P2) to new and total PP in the SCS.

Compared with seasonal variations, the year-to-year variability in the SCS is relatively small, and often it is difficult to discern the underlying causes of such changes because of the scarcity of systematic observations on a basin scale. Year-to-year changes in physical and biological conditions, such as upwelling intensity and nutrient concentrations, need to be investigated further, to explain the modelled and observed variation of biological productivity and export flux.

Summary

A Pacific basin-wide three-dimensional physical–biogeochemical model has been developed and used to evaluate seasonal and interannual variation of biological productivity and export flux in the SCS for the period 1990–2004. The ROMS–CoSiNE model can reproduce some of the observations conducted at the SEATS site, including seasonal and interannual variations of SST and SSS, and vertical profiles of nitrate, silicate, Chl *a*, and PP. The main results from this modelling study are summarized below.

(i) In the SCS, the annual mean PP is low, except for a few upwelling-dominated regions, such as the Vietnam coast in summer and the western side of Luzon Island in winter. The modelled PP and its variability agree well with previous modelling and observational results (Liu *et al*., 2002; Chen, 2005). The dominant seasonal variation of PP responds to the seasonal changes of the windforcing associated with the East Asia monsoon.

(ii) The seasonal variation in new production is in the range 55–76 mg C m^{-2} d^{-1}, much lower than the variability in PP (156–386 mg C m^{-2} d^{-1}). This indicates that strong seasonal variations in PP are mainly caused by regenerated production in the SCS. The modelled annual mean *f*-ratio for

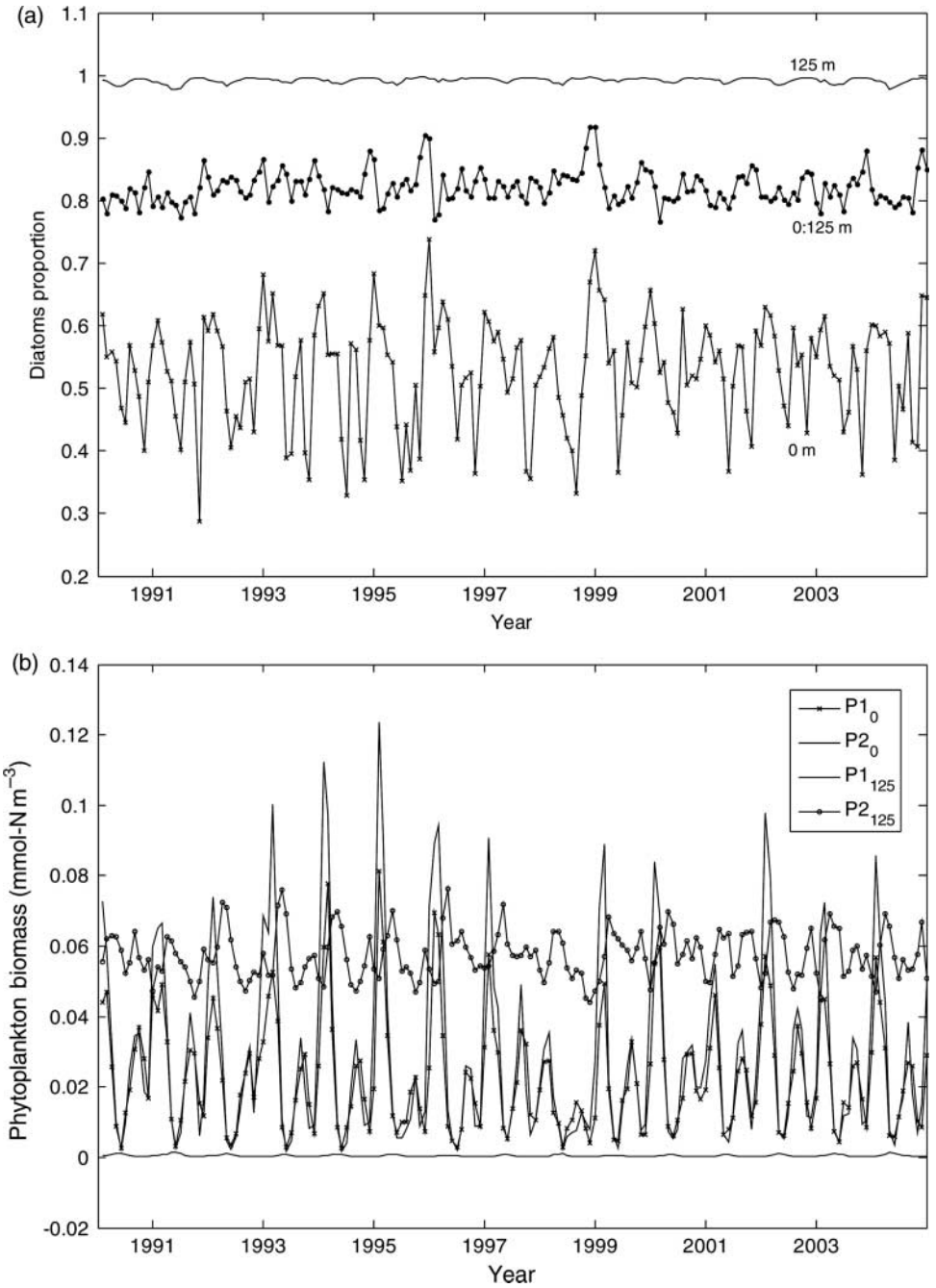

Figure 10. Interannual variability in (a) proportion of diatoms at the surface (line with crosses), diatoms at 125 m (solid line), and depth-integrated diatoms at 0–125 m (line with dots); and (b) phytoplankton biomass ($P1_0$ and $P2_0$, small phytoplankton and diatoms, respectively, at the surface; $P1_{125}$ and $P2_{125}$, small phytoplankton and diatoms, respectively, at 125 m).

the entire SCS is 0.33, and the regenerated ammonium uptake accounts for two-thirds of the total PP.

(iii) The annual mean POC export flux across the 125-m depth contour is 46.5 mg C m^{-2} d^{-1}, comparable with the estimated POC flux derived from sediment trap observations and model output (Liu *et al.*, 2002). The modelled export ratio (the *e*-ratio = POC flux at 125 m/IPP) is 0.24.

(iv) Compared with the seasonal cycle, the year-to-year variation of biological productivity in the SCS is weak. The large phytoplankton group tends to be dominant over the smaller easily grazed phytoplankton and plays an important role in determining the interannual variability of primary and new production.

These findings have shed new light on the seasonal and interannual variations in IPP, INP, and POC export flux in the SCS. Although the results suggest some noteworthy trends and intriguing issues, they need to be confirmed with more observations, especially through long-term data. In addition, the model needs to be constrained and evaluated with more physical and biogeochemical observations, especially for the simultaneous

observations of biogeochemical variables and environmental factors. In future, higher model resolution and river discharges are required to resolve the dynamics of the vast shallow region in the SCS appropriately.

Acknowledgements

This research was supported by a NASA grant (NNG04GM64G) and NSFC (90711006) to FC. NSFC grants 40531006 and 40676019 also supported part of our effort in writing up the manuscript. We thank K. K. Liu, C. M. Tseng, and other scientists for sharing the SEATS observational data, Lei Shi at the University of Maine for helping us process some of the model results, and Yi Chao at JPL/NASA for sharing the ROMS circulation model configuration for the Pacific Ocean. Finally, we acknowledge the inputs of Elizabeth North and Franz Mueter, the co-editors of this suite of papers, and four reviewers, whose comments greatly improved the contents of the paper.

References

Anderson, L. A., and Sarmiento, J. L. 1994. Redfield ratios of remineralization determined by nutrient data analysis. Global Biogeochemical Cycles, 8: 65–80.

Bidigare, R. R., and Ondrusek, M. E. 1996. Spatial and temporal variability of phytoplankton pigment distributions in the central equatorial Pacific Ocean. Deep Sea Research II, 43: 809–833.

Chai, F., Barber, R. T., and Lindley, S. T. 1996. Origin and maintenance of high nutrient condition in the equatorial Pacific. Deep Sea Research II, 42: 1031–1064.

Chai, F., Dugdale, R. C., Peng, T. H., Wilkerson, F. P., and Barber, R. T. 2002. One dimensional ecosystem model of the equatorial Pacific upwelling system. 1. Model development and silicon and nitrogen cycle. Deep Sea Research II, 49: 2713–2745.

Chai, F., Jiang, M., Barber, R. T., Dugdale, R. C., and Chao, Y. 2003. Interdecadal variation of the transition zone chlorophyll front, a physical–biological model simulation between 1960 and 1990. Journal of Oceanography, 59: 461–475.

Chai, F., Jiang, M. S., Chao, Y., Dugdale, R. C., Chavez, F., and Barber, R. T. 2007. Modeling responses of diatom productivity and biogenic silica export to iron enrichment in the equatorial Pacific Ocean. Global Biogeochemical Cycles, 21: GB3S90. doi:10.1029/2006GB002804.

Chai, F., Xue, H., and Shi, M. 2001a. General circulation and its seasonal variation in the northern and central South China Sea. *In* Oceanography in China. 13. South China Sea Circulation Modeling and Observations, pp. 39–56. Ed. by H. Xue, F. Chai, and J. Xu. China Ocean Press, Beijing. 254 pp.

Chai, F., Xue, H., and Shi, M. 2001b. Formation and distribution of upwelling and downwelling in the South China Sea. *In* Oceanography in China. 13. South China Sea Circulation Modeling and Observations, pp. 117–128. Ed. by H. Xue, F. Chai, and J. Xu. China Ocean Press, Beijing. 254 pp.

Chao, S. Y., Shaw, P. T., and Wu, S. Y. 1996. *El Niño* modulation of the South China Sea circulation. Progress in Oceanography, 38: 51–93.

Chavez, F. P., Buck, K. R., Coale, K. H., Martin, J. H., DiTullio, G. R., Welshmeyer, N. A., Jacobson, A. C., *et al.* 1991. Growth rates, grazing, sinking and iron limitation of equatorial Pacific phytoplankton. Limnology and Oceanography, 36: 1816–1833.

Chen, C. C., Shiah, F. K., Chung, S. W., and Liu, K. K. 2006. Winter phytoplankton blooms in the shallow mixed layer of the South China Sea enhanced by upwelling. Journal of Marine Systems, 59: 97–110.

Chen, C. T. A., Hou, W. P., Gamo, T., and Wang, S. L. 2006. Carbonate-related parameters of subsurface waters in the West Philippine, South China and Sulu Seas. Marine Chemistry, 99: 151–161.

Chen, C. T. A., Wang, S. L., Wang, B. J., and Pai, S. C. 2001. Nutrient budgets for the South China Sea basin. Marine Chemistry, 75: 281–300.

Chen, Y. L. L. 2005. Spatial and seasonal variation of nitrate-based new production and primary production in the South China Sea. Deep Sea Research I, 52: 319–340.

Chu, P. C., and Fan, C. W. 2001. A low salinity cool-core cyclonic eddy detected northwest of Luzon during the South China Sea Monsoon Experiment (SCSMEX) in July 1998. Journal of Oceanography, 57: 549–563.

Coale, K. H., Johnson, K. S., Fitzwater, S. E., Gordon, R. M., Tanner, S., Chavez, F. P., Ferioli, L., *et al.* 1996. A massive phytoplankton bloom induced by an ecosystem-scale iron fertilization experiment in the equatorial Pacific Ocean. Nature, 383: 495–501.

Dippner, J. W., Nguyen, K. V., Hein, H., Ohde, T., and Loick, N. 2007. Monsoon-induced upwelling off the Vietnamese coast. Ocean Dynamics, 57: 46–62.

Dugdale, R. C., Barber, R. T., Chai, F., Peng, T. H., and Wilkerson, F. P. 2002. One dimensional ecosystem model of the equatorial Pacific upwelling system. 2. Sensitivity analysis and comparison with JGOFS EqPac data. Deep Sea Research II, 49: 2746–2762.

Fang, G., Chen, H., Wei, Z., Wang, Y., Wang, X., and Li, C. 2006. Trends and interannual variability of the South China Sea surface winds, surface height, and surface temperature in the recent decade. Journal of Geophysical Research, 111: C11S16. doi:10.1029/2005JC003276.

Fang, G., Susanto, D., Soesilo, I., Zheng, Q., Qiao, F., and Wei, Z. 2005. A note on the South China Sea shallow interocean circulation. Advances in Atmospheric Sciences, 22: 946–954.

Fujii, M., Yoshie, N., Yamanaka, Y., and Chai, F. 2005. Simulated biogeochemical responses to iron enrichments in three high nutrient, low chlorophyll (HNLC) regions. Progress in Oceanography, 64: 307–324.

Gardner, W. D., Mishonov, A. V., and Richardson, M. J. 2006. Global POC concentrations from *in-situ* and satellite data. Deep Sea Research II, 53: 718–740.

Geider, R. J., MacIntyre, H. L., and Kana, T. M. 1998. A dynamic regulatory model of phytoplankton acclimation to light, nutrients and temperature. Limnology and Oceanography, 43: 679–694.

Gong, G. C., Liu, K. K., Liu, C. T., and Pai, S. C. 1992. The chemical hydrography of the South China Sea west of Luzon and a comparison with the West Philippine Sea. Terrestrial, Atmospheric and Oceanic Sciences, 3: 587–602.

He, Y. H., Guan, C. H., and Gan, Z. J. 1997. Interannual and interdecadal variations in heat content of the upper ocean of the South China Sea. Advances in Atmospheric Sciences, 14: 271–276.

Jennerjahn, T. C., Liebezeit, G., Kempe, S., Xu, L. Q., Chen, W. B., and Wong, H. K. 1992. Particle flux in the northern South China Sea. *In* Marine Geology and Geophysics of the South China Sea, pp. 228–235. Ed. by X. Jin, H. R. Kudrass, and G. Pautot. China Ocean Press, Beijing. 266 pp.

Kalnay, E., Kanamitsu, M., Kistler, R., Collins, W., Deaven, D., Gandin, L., Iredell, M., *et al.* 1996. The NCEP/NCAR 40-year reanalysis project. Bulletin of the American Meteorological Society, 77: 437–470.

Kuo, N. J., Zheng, Q., and Ho, C. R. 2004. Response of Vietnam coastal upwelling to the 1997–1998 ENSO event observed by multisensor data source. Remote Sensing of the Environment, 89: 106–115.

Landry, M. R., Barber, T., Bidigare, R. R., Chai, F., Coale, K. H., Dam, H. G., Lewis, M. R., *et al.* 1997. Iron and grazing constraints on primary production in the central equatorial Pacific: an EqPac synthesis. Limnology and Oceanography, 42: 405–418.

Landry, M. R., Constantinou, J., and Kirshtein, J. 1995. Microzooplankton grazing in the central equatorial Pacific during February and August, 1992. Deep Sea Research II, 42: 657–672.

Large, W., and Pond, S. 1982. Sensible and latent heat flux measurements over the ocean. Journal of Physical Oceanography, 12: 464–482.

Large, W. G., McWilliams, J. C., and Doney, S. C. 1994. Oceanic vertical mixing: a review and a model with a non-local K-profile boundary layer parameterization. Reviews of Geophysics, 32: 363–403.

Laws, E. A., Falkowski, P. G., Smith, W. O., Ducklow, H., and McCarthy, J. J. 2000. Temperature effects on export production in the open ocean. Global Biogeochemical Cycles, 14: 1231–1246.

Liang, W. D., Tang, T. Y., Yang, Y. J., Ko, M. T., and Chuang, W. S. 2003. Upper ocean currents around Taiwan. Deep Sea Research II, 50: 1085–1105.

Liu, K. K., Chao, S. Y., Shaw, P. T., Gong, G. C., Chen, C. C., and Tang, T. Y. 2002. Monsoon-forced chlorophyll distribution and primary production in the South China Sea: observations and a numerical study. Deep Sea Research I, 49: 1387–1412.

Liu, K. K., Kao, S. J., Hu, H. C., Chou, W. C., Hung, G. W., and Tseng, C. M. 2007. Carbon isotopic composition of suspended and sinking particulate organic matter in the northern South China Sea—from production to deposition. Deep Sea Research II. doi:10.1016/j.dsr2.2007.05.010.

Martin, J. H., Knauer, G. A., Karl, D. M., and Broenkow, W. W. 1987. VERTEX: carbon cycling in the north Pacific. Deep Sea Research I, 34: 267–285.

Metzger, E. J., and Hurlburt, H. E. 1996. Coupled dynamics of the South China Sea, the Sulu Sea, and the Pacific Ocean. Journal of Geophysical Research, 101C: 12331–12352.

Metzger, E. J., and Hurlburt, H. E. 2001. The importance of high horizontal resolution and accurate coastline geometry in modeling South China Sea inflow. Geophysical Research Letters, 28: 1059–1062.

Ning, X., Chai, F., Xue, H., Cai, Y., Liu, C., Zhu, G., and Shi, J. 2004. Physical–biological oceanographic coupling influencing phytoplankton and primary production in the South China Sea. Journal of Geophysical Research, 109: C10005. doi:10.1029/2004JC002365.

Ocean Climate Laboratory National Oceanographic Data Center. 2002. World Ocean Atlas 2001. http://www.nodc.noaa.gov.

Qu, T. D. 2000. Upper-layer circulation in the South China Sea. Journal of Physical Oceanography, 30: 1450–1460.

Rong, Z. R., Liu, Y. G., Zong, H. B., and Cheng, Y. C. 2006. Interannual sea level variability in the South China Sea and its response to ENSO. Global and Planetary Change, 55: 257–272.

Shaw, P. T., Chao, S. Y., Liu, K. K., Pai, S. C., and Liu, C. T. 1996. Winter upwelling off Luzon in the northeastern South China Sea. Journal of Geophysical Research, 101C: 16435–16448.

Shchepetkin, A., and McWilliams, J. C. 1998. Quasi-monotone advection schemes based on explicit locally adaptive dissipation. Monthly Weather Review, 126: 1541–1580.

Shchepetkin, A. F., and McWilliams, J. C. 2003. A method for computing horizontal pressure-gradient force in an ocean model with a non-aligned vertical coordinate. Journal of Geophysical Research, 108: 3090. doi:10.1029/2001JC001047.

Smetacek, V. 1985. The annual cycle of Kiel bight plankton: a long term analysis. Estuaries, 8: 145–157.

Straub, K. H., Kiladis, G. N., and Ciesielski, P. E. 2006. The role of equatorial waves in the onset of the South China Sea summer monsoon and the demise of *El Niño* during 1998. Dynamics of Atmospheres and Oceans, 42: 216–238.

Su, J. L. 2004. Overview of the South China Sea circulation and its influence on the coastal physical oceanography outside the Pearl River Estuary. Continental Shelf Research, 24: 1745–1760.

Takano, K., Harashima, A., and Namba, T. 1998. A numerical simulation of the circulation in the South China Sea—preliminary results. Acta Oceanographica Taiwanica, 37: 165–185.

Tang, D. L., Kawamura, H., Dien, T. V., and Lee, M. A. 2004. Offshore phytoplankton biomass increase and its oceanographic causes in the South China Sea. Marine Ecology Progress Series, 268: 31–41.

Thomas, W. H., and Dodson, A. N. 1972. On nitrogen deficiency in tropical Pacific oceanic phytoplankton. 2. Photosynthetic and cellular characteristics of a chemostat-grown diatom. Limnology and Oceanography, 17: 515–523.

Tseng, C. M., Wong, G. T. F., Chou, W. C., Lee, B. S., Sheu, D. D., and Liu, K. K. 2007. Temporal variations in the carbonate system in the upper layer at the SEATS station. Deep Sea Research II. doi:10.1016/j.dsr2.2007.05.003.

Tseng, C. M., Wong, G. T. F., Lin, I. I., Wu, C. R., and Liu, K. K. 2005. A unique seasonal pattern in phytoplankton biomass in low-latitude waters in the South China Sea. Geophysical Research Letters, 32: L08608. doi:10.1029/2004GL022111.

Wang, G. H., Su, J. L., and Qi, Y. Q. 2005. Advances in studying mesoscale eddies in South China Sea. Advance in Earth Sciences, 20: 882–886.

Wang, X., and Chao, Y. 2004. Simulated sea surface salinity variability in the tropical Pacific. Geophysical Research Letters, 31: L02302. doi:10.1029/2003GL018146.

Wong, G. T. F., Ku, T. L., Mulholland, M., Tseng, C. M., and Wang, D. P. 2007. The SouthEast Asian Time-series Study (SEATS) and the biogeochemistry of the South China Sea—an overview. Deep Sea Research II, 54: 1434–1447.

Wu, C. R., and Chang, C. W. J. 2005. Interannual variability of the South China Sea in a data assimilation model. Geophysical Research Letters, 32: L17611. doi:10.1029/2005GL023798.

Wu, C. R., Shaw, P. T., and Chao, S. Y. 1998. Seasonal and interannual variations in the velocity field of the South China Sea. Journal of Oceanography, 54: 361–372.

Wyrtki, K. 1961. Physical oceanography of the Southeast Asian waters. University of California, NAGA Report, 2. 195 pp.

Xie, S. P., Xie, Q., Wang, D. X., and Liu, W. T. 2003. Summer upwelling in the South China Sea and its role in regional climate variations. Journal of Geophysical Research, 108C: 3261. doi: 2003JC001867.

Xue, H., Chai, F., Pettigrew, N., Xu, D., Shi, M., and Xu, J. 2004. Kuroshio intrusion and the circulation in the South China Sea. Journal of Geophysical Research, 109C: 02017. doi:10.1029/2002JC001724.

Yin, K. D. 2002. Monsoonal influence on seasonal variations in nutrients and phytoplankton biomass in coastal waters of Hong Kong in the vicinity of the Pearl River estuary. Marine Ecology Progress Series, 245: 111–122.

Zhao, H., and Tang, D. L. 2007. Effect of 1998 *El Niño* on the distribution of phytoplankton in the South China Sea. Journal of Geophysical Research, 112C: 02017. doi:10.1029/2006JC003536.

doi:10.1093/icesjms/fsn219